Fast isotropic adatom diffusion on Ge(105) dot facets

F. Montalenti,[1,*] D. B. Migas,[1] F. Gamba,[1] and Leo Miglio[1]
[1]*INFM and L-NESS, Dipartimento di Scienza dei Materiali della Università degli Studi di Milano-Bicocca, Via Cozzi 53, I-20125 Milano, Italy*
(Received 31 May 2004; published 16 December 2004)

We investigate adatom self-diffusion on the rebonded step (RS) reconstructed Ge(105) surface. Activation energies for several paths are computed *ab initio* by applying the nudged elastic band method and used as input parameters for kinetic Monte Carlo simulations. We show that the RS reconstruction strongly influences adatom kinetics, which turns out to be fast at typical experimental temperatures, along both [010] and $[\bar{5}01]$ directions. The influence of strain on diffusion is also investigated. Our results are shown to be relevant for a better understanding of the growth modality of Ge pyramids on Si(001).

DOI: 10.1103/PhysRevB.70.245315 PACS number(s): 68.35.Fx, 68.47.Fg, 68.43.Bc

I. INTRODUCTION

Deposition of Ge on Si substrates produces elastic-energy accumulation due to the sizable lattice misfit. Under suitable experimental conditions, strain is released via the formation of three-dimensional islands of nanometric size.[1,2] Due to the possible technological applications and to the fascinating physics underlying such phenomena, Ge/Si (and SiGe alloys grown on Si substrates) have been the object of several experimental and theoretical studies (for a review, see Refs. 3 and 4). The importance of the (105) surface in Ge/Si(001) systems was clearly demonstrated by the STM images of Mo *et al.*,[1] showing Ge huts clusters bounded by {105} facets fast growing on Si(001). Since then, several other experimental evidences revealed how easily {105} orientations appear in Ge or Si_xGe_{1-x} growth on Si(001).[4–7] Very recently, it has been shown that a rebonded-step (RS) reconstruction[8] is energetically favored[9–11] on the Ge(105) surface. In particular, it was demonstrated that the RS reconstruction actually takes place at Ge pyramids facets,[9] and that it plays a key role in determining the dots stability.[9,12] Such a reconstruction dramatically changes the as-cut geometry, virtually eliminating the step stucture, flattening the (105) surface, and causing enhanced stability under compressive strain.[11–14] If the above mentioned references provide detailed theoretical information about surface thermodynamics, kinetics at the RS(105) surface is still unexplored. Since kinetics often plays a key role in determining the morphology of growing films,[15,16] understanding how and how fast atoms move at the RS(105) surface should be regarded as a crucial step towards a comprehensive microsopic modeling of the observed dot growth modes.[1,2,6,7] In this paper we investigate isolated Ge adatom self-diffusion on the Ge RS(105) surface. Our aim, in particular, is to understand what is the role played by the RS reconstruction in influencing kinetics. If diffusion at the (105) surface, as cut, is expected to reflect the anisotropy typical of vicinal surfaces, where step crossing is hindered by step barriers,[16] it is interesting to see how deeply can the RS reconstruction change this scenario. In order to make quantitative predictions useful for further modeling, we evaluate the tracer diffusion coefficient along the $[\bar{5}01]$ and [010] directions, corresponding to the base-to-top and to the lateral direction, respectively, in a {105} pyramid facet. To this goal, by following an *ab initio* approach, we first determine the location of the adatom local minima on the surface. Activation energies, relative to paths connecting neighbouring minima, are subsequently computed. After evaluating the corresponding rates using the harmonic approximation to the transition state theory[17] (hTST), we run kinetic Monte Carlo simulations, ultimately yielding the diffusion coefficients. While results are initially found for an unstrained Ge(105)RS surface (as found at the top of {105} Ge dots), the whole set of calculations is then repeated for a Ge(105)RS surface under a ~4% compressive strain, in order to mimic the typical conditions found close to the Ge/Si(001) dots base, where the lattice parameter approaches the Si-bulk one.[4]

The paper is organized in the following way. At the beginning of Sec. II we describe the methodology used to locate Ge adatom minima, and to compute diffusion barriers. In Sec. II A the typical geometry of the adsorption sites is reported, while the activation energies values are introduced in Sec. II B. Kinetic Monte Carlo trajectories and diffusion coefficients are described in Sec. III. The effects of compressive strain on diffusion is tackled in Sec. IV, while in Sec. V we link the present results to observed Ge pyramid growth modes, and to previous modeling, before summarizing the main points discussed in the paper.

II. LOCAL MINIMA AND ACTIVATION ENERGIES

All the diffusion barriers reported in this paper were computed *ab initio*, by applying the ultrasoft pseudopotential method, as implemented in the VASP code.[18–21] The local density approximation of Ceperley and Alder as parametrized by Perdew and Zunger[22] was utilized. The RS reconstructed (105) surface configuration was considered as a periodic arrangement of slabs separated by 12 Å of vacuum. Each slab was composed of 14 ML. All of the atoms were allowed to relax, but the four bottom layers were kept fixed to bulk positions, while dangling bonds at the lower surface were saturated with hydrogen atoms. We used an energy cutoff of 200 eV. The in-plane lattice parameter $a_{\|}$ was set to $a_{\|}=5.6567$ Å (except for the results reported in Sec. IV,

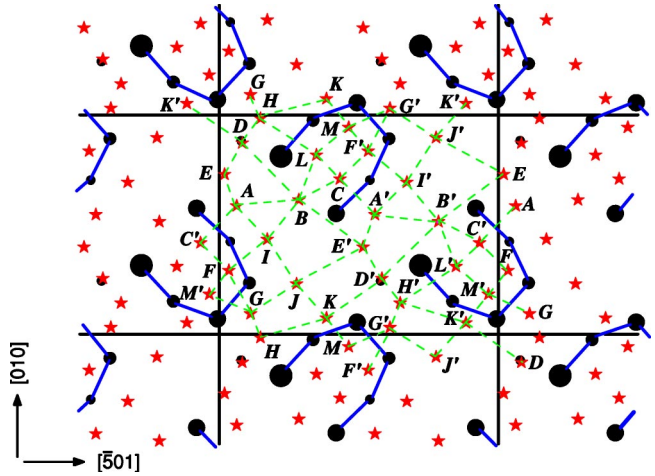

FIG. 1. Top view of the RS reconstructed Ge(105) surface. The central rectangular region represents the surface unit cell (14.422 $\times$11.31 Å). Solid circles stand for surface atoms and the circle's size corresponds to the atom position along [105]. The boundaries of the typical HS structures are drawn with thick solid lines. The adsorption sites are indicated by stars and named by capital letters, while possible diffusion paths are traced with dashed lines.

where a $\sim$4.2% reduction in $a_{\parallel}$ was considered), corresponding to the experimental Ge-bulk equilibrium value (close to the LDA one $a_{\parallel}$=5.623 Å), while a $4\times5\times1$ grid of Monkhorst-Pack points turned out to be sufficient to guarantee results convergence. In finding local minima, atomic relaxations, performed by using a conjugate gradient algorithm, were stopped when the forces on the atoms were less than 0.01 eV/Å. In order to compute the adatom diffusion barriers, we have used the nudged elastic band (NEB) method,[23] with the inclusion of the climbing-image refinement,[24] which allows for accurate saddle-point energy estimates. Due to the very high number of activation energies involved in our calculations, geometry optimizations of the saddle points were stopped by using a less restrictive criterium (forces less than 0.08 eV/Å). Still, convergence checks performed on two randomly selected saddle-point configurations yielded differences in barriers less than 0.02 eV.

A. Local minima: results

In order to investigate diffusion on Ge(105), we first identified the adatom binding sites. We probed with a Ge adatom the RS reconstructed Ge(105) surface by using a 7×6 grid of initial adatom surface coordinates, and by minimizing the energy of the system in each position. The geometry of the RS surface, already described in previous papers (for example, see Refs. 9, 11, and 12), displays an array of horseshoe (HS-) like structures, sketched in Fig. 1.

Notice that the surface unit cell (central rectangular area in Fig. 1) is relatively large with respect to the one of the 2×1 Ge(001), where many nonequivalent binding sites were reported,[25] so that a proliferation of possible local minima is expected. Indeed, we found 13 nonequivalent binding sites resulting in a total of 26 sites in the cell, because of the twofold rotational symmetry axis along the [010] direction. The 26 minima are indicated by stars and letters ($A, B, \ldots, M$ for the first set, $A', B', \ldots, M'$ for the symmetrically equivalent ones) in Fig. 1. Few additional local minima emerged during the calculation of the diffusion barriers. All of them, however, turned out to be extremely shallow, and are not included in Fig. 1. The differences in binding energy are summarized in Table I (upper row). The best adsorption sites turn out to be B (B') and D (D'), extremely close in energy. While in Fig. 1 all minima are represented at once, and HS structures are drawn in their unperturbed, clean surface configuration, a better idea of the adatom-surface binding can be inferred from Fig. 2, where the unperturbed HS structure (upper panel) is shown together with the lowest-energy sites, i.e., B (central panel) and D (lower panel). The presence of the adatom in B or in D is particularly stabilizing since it saturates one dangling bond on both adjacent dimers, similarly to what happens at the (001) surface (see Fig. 1 in Ref. 25). While in the B and D configurations the adatom does not produce major distortions in the HS structure (changes in the tilting of the dimers adjacent to the adatom, though, can be spotted in Fig. 2), this is not the case when the sites A, C, E, or L are occupied, leading to a breaking in one of the bonds of the HS structure. As it is illustrated in Fig. 3, the presence of the adatom in A (upper panel) pulls one of the atoms of the more distant HS towards the HS stucture to which the adatom is attached with two bonds. A similar change occurs in the E configuration, where, however, the adatom sticks to the lower HS with a single bond. In L (and, similarly, in C), on the other hand, the adatom binds to two HS atoms, breaking their bond. The sizable stretching of some of the HS bonds in the clean-surface configuration[12] surely helps in causing the here observed bond-breaking processes.

B. Activation energies: results

In order to scan for possible jumplike diffusion mechanisms (more complex events, such as exchanges between the adatom and a surface atom were not investigated), we have calculated the energy barrier along paths joining neighboring minima. In Fig. 1, dashed lines are drawn between all the local-minima pairs for which the activation energy was

TABLE I. Difference in energy (eV) between the various minima sketched in Fig. 1, and the best adsorption site. Upper row values refer to the Ge in-plane lattice parameter (a_{Ge}), while the lower row reports the results obtained at a_{Si}. The lowest-energy site is B for $a_{\parallel}=a_{\mathrm{Ge}}$ and D for $a_{\parallel}=a_{\mathrm{Si}}$.

	E_A	E_B	E_C	E_D	E_E	E_F	E_G	E_H	E_I	E_J	E_K	E_L	E_M
a_{Ge}	0.178	0.000	0.111	0.007	0.278	0.463	0.401	0.323	0.248	0.532	0.340	0.368	0.436
a_{Si}	0.289	0.011	0.228	0.000	0.574	0.507	0.377	0.301	0.339	0.453	0.433	0.546	0.474

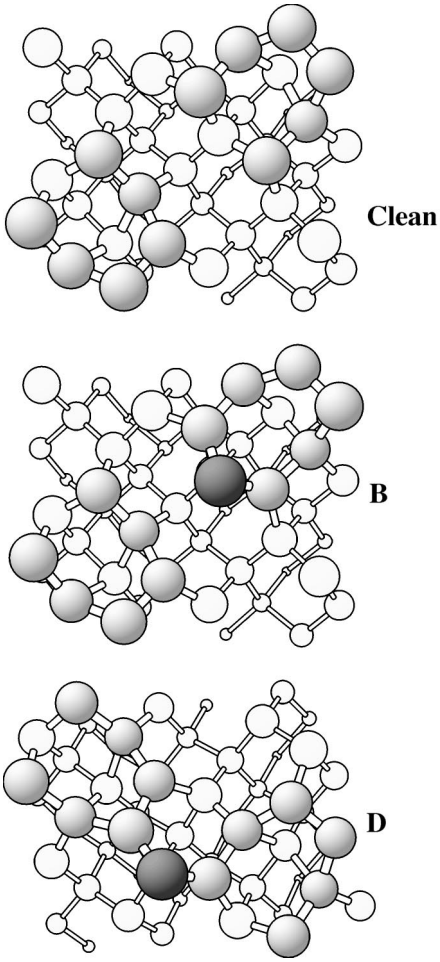

FIG. 2. Top view of the clean-surface configuration (upper panel) and of the two deepest adatom minima *B* and *D* (labeling is according to Fig. 1), as optimized for $a_{\parallel}=a_{\mathrm{Ge}}$. Substrate atoms are represented by empty circles, the HS structures by gray circles, while a black circle is used for the adatom. In representing minimum *D*, where the adatom lays between two HS, the unit cell was recentered with respect to Fig. 1. Larger circles are used for atoms closer to the observer. Bonds are displayed between pairs of atoms distanced by less than ~2.73 Å (bulk distance: ~2.45 Å).

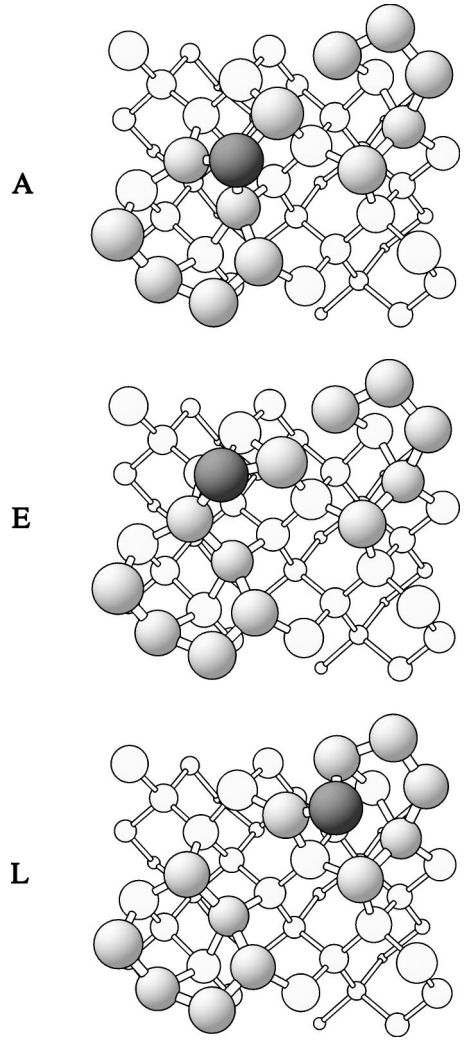

FIG. 3. Top view of the *A* (upper panel), *E* (central), and *L* (lower) adatom-minima configurations, as optimized for $a_{\parallel}=a_{\mathrm{Ge}}$. Atoms are displayed following the same criteria described in the caption of Fig. 2.

evaluated. Barriers were computed using the NEB method, which is described with many details in several publications (see, e.g., Refs. 23, 24, and 26). Here we simply recall that the method allows one to find the saddle point separating adjacent minima without knowing *a priori* the multidimensional reaction coordinate. This goal is achieved by building a chain of images laying between the initial and final minimum (which are the initial and final image), by artificially connecting the neighboring ones with springs, and by finally minimizing an appropriate effective force acting on each image. In our NEB calculations, the chain of states was initialized by linearly interpolating the initial and the final configurations. Depending on the path length, five or seven NEB images were used. After convergence of the NEB procedure, due to the complexity of the (105)RS geometry, diffusion paths between adjacent minima generally turned out to be nonlinear. Similarly, saddle-point configurations were not found in symmetric positions between the minima.

Due to the very high number of activation energies computed in this work, we shall not display the various saddle-point configurations. Simply, we shall focus on the typical activation-energy values, which are reported in Table II (see the $a_{\parallel}=a_{\mathrm{Ge}}$ rows). The energy barrier to move from one of the 26 minima *P* to a neighbor *Q* is indicated by E_{PQ} in Table II. The reverse barrier to move from *Q* to *P* can be computed using the obvious relation $E_{QP}=E_{PQ}-(E_Q-E_P)$, where E_P and E_Q, reported in Table I, are the energies of the *P* and *Q* minima. Finally, if point *P* and/or *Q* are not reported in Table II, but their symmetric ones are (P',Q'), one should recall that $E_{P,Q}=E_{P',Q'}$ and $E_{P',Q}=E_{P,Q'}$. These simple rules allow one to know the barrier values for every path indicated in Fig. 1. As is clearly seen in Table II, the activation energies for the individual mechanisms are distributed over a wide range of values, ranging from several meV to eV. This lack of uniformity reflects the complexity of the RS(105) unit cell, already evident from the local-minimum analysis. In the next section, we shall model long time-scale adatom diffusion by KMC simulations. The trajectory analy-

TABLE II. Activation energies (eV) for adatom diffusion between neighbouring sites at both $a_{\|}=a_{\mathrm{Ge}}$ and $a_{\|}=a_{\mathrm{Si}}$.

	E_{DH}	$E_{DK'}$	E_{DE}	E_{DB}	E_{BA}	E_{BI}	$E_{BE'}$	E_{BC}	E_{BL}	E_{JG}	E_{JI}	E_{JK}	$E_{JE'}$
a_{Ge}	0.517	1.019	0.534	0.789	0.677	0.696	0.706	0.582	0.582	0.238	0.030	0.242	0.495
a_{Si}	0.690	0.728	0.610	0.860	0.904	0.948	1.757	0.736	0.736	0.253	0.102	0.137	0.524

	E_{FI}	E_{FG}	$E_{FM'}$	$E_{FC'}$	E_{AE}	$E_{AC'}$	E_{AI}	$E_{MG'}$	E_{MK}	E_{ML}	E_{HK}	E_{HG}	E_{HL}	E_{CL}
a_{Ge}	0.126	0.281	0.444	0.098	0.358	0.132	0.327	0.308	0.061	0.181	0.327	0.091	0.310	0.473
a_{Si}	0.177	0.302	0.553	0.059	0.412	0.254	0.203	0.337	0.116	0.352	0.354	0.084	0.799	0.630

sis will help in revealing which of the events displayed in Fig. 1 are more relevant in determining adatom diffusion.

III. KINETIC MONTE CARLO SIMULATIONS

Once the activation energies for individual processes are known, the corresponding diffusion rates can be immediately evaluated using hTST. In particular, if E_i is the activation energy for a given mechanism i, the corresponding rate ν_i can be estimated using the Arrhenius relation

$$\nu_i = \nu_i^0 \exp(-E_i/k_B T), \tag{1}$$

where ν_i^0 is a frequency prefactor, T the substrate temperature, and k_B the Boltzmann constant. In the present calculations, we have estimated the diffusion rates by using the activation energy values reported in Table II (see the $a_{\|}=a_{\mathrm{Ge}}$ row), and by setting all frequency prefactors ν_i^0 to the standard value of 10^{13} s^{-1} (a popular choice in modeling diffusion at semiconductor surfaces, see Refs. 27 and 28), avoiding computationally expensive prefactor evaluations. In the presence of several alternative diffusion paths characterized by very different activation energies (see Table II), the simple knowledge of the individual rates does not allow one to understand the overall diffusive behavior of the system. Trajectories representative of the state-to-state dynamics are needed. In order to generate such trajectories, we have simulated adatom diffusion across several unit cells by plugging the individual rates into a kinetic Monte Carlo (KMC) code. KMC is nowadays considered to be a standard simulation technique. Seminal works on KMC can be found in Refs. 29–31. Here we quickly summarize some general apsects of KMC simulations which we exploited in our calculations. In each state S visited by the system, a list of possible mechanisms and rates to exit from S is provided. If $\nu_{\mathrm{tot}}^S=\Sigma_i \nu_i^S$ is the total rate for diffusing out of S, a probability $p_j^S=\nu_j^S/\nu_{\mathrm{tot}}^S$ is assigned to each individual mechanism that can take the system out of S. Once one of the possible mechanisms has been chosen with the correct statistical weight (p_j^S), the system is moved into a new state determined by the particular mechanism, the simulation time is advanced by extracting the escape time t from the distribution $f(t)dt=\nu_{\mathrm{tot}}^S \exp-(\nu_{\mathrm{tot}}^S t)dt$, and the procedure is repeated until the desired time scale is reached. If the list of rates is complete, and rates are computed exactly, KMC simulations allow one to simulate exact state-to-state dynamics.

In Fig. 4, we show three typical KMC trajectories corresponding to a temporal evolution of 0.1 μs, at $T=600$ K (left panel), $T=700$ K (central), and $T=800$ K (right), a typical temperature used in Ge dots growth on Si(001).[9] In the figure, the size of the portion of the cell represented is scaled in order to show the whole trajectory. As it is particularly clear in the $T=800$ K case, where a larger number of events is displayed, diffusion appears to be rather isotropic. The overall trajectories are given by the combination of many different atomic mechanisms. While it is impossible to relate the diffusive process to a single path, some general features of the atomic motion can be inferred. Atoms move by repeatedly entering and exiting from the HS structures, while positions within the trenches separating such structures are rather rare. This behavior can be understood by looking at the minima location (Fig. 1), at their energy (Table I) and at the typical barriers (Table II). Local minima are concentrated in the close surrounding and inside HS structures, where the adatom can fill more easily surface dangling bonds. Once the adatom reaches the best adsorption site, B, the lowest barrier mechanism corresponds to a jump into the HS structure, for example, to site L, from where it easily reaches M. At this point exiting and reentering in the HS is extremely easy. Moving from M to K only requires to surmount $E_{MK}\sim 60$ meV. The reverse path is also characterized by a very low barrier ($E_{KM}\sim 0.16$ eV), so that KMC trajectories are characterized by long $M\rightarrow K\rightarrow M$ sequences. In this event, the adatom moves from one minimum to the other without breaking bonds, displaying a rotationlike motion around one of the HS bonds (see Fig. 1). As is clear from Table II, other similar low-barrier events take place. Notice, however, that

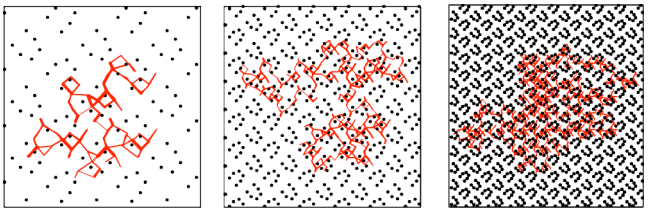

FIG. 4. Adatom KMC trajectories at three different temperatures: 600 (left), 700 (central), and 800 K (right panel). The simulation time is of 0.1 μs. Surface atoms composing the HS structures, oriented as in Fig. 1 (the vertical direction is [010], the horizontal $[\bar{5}01]$) are represented with full circles. The adatom trajectory is traced with a solid line (red, in the electronic version of the paper). A thicker line is used when multiple transitions between the same pair of minima occurred (not visible at $T=800$ K, due to the very high number of processes displayed).

such events, although very frequent, do not allow for a truly diffusive motion, which requires the adatom to move between different HS, surmounting higher barriers (such as E_{BA}, E_{BI}, or E_{DE}).

The above observed isotropic diffusive behavior is an important consequence of the RS reconstruction. The (105) surface, as cut from the bulk, is a typical vicinal surface characterized by a set of parallel steps.[9,11] Diffusion across the steps is likely to be slower since step barriers need to be surmounted (see, e.g., Ref. 16). So, in the absence of the reconstruction, one would predict the [010] direction (vertical in Fig. 4) to be preferential for atomic motion. As explicitly demonstrated by our results, the RS reconstruction changes completely the diffusion scenario. In order to clarify further this issue, we have computed the adatom diffusion coefficient in the [010] and $[\bar{5}01]$ directions. To this goal, we have estimated the time-dependent mean square displacements $\langle X^2(t)\rangle$ and $\langle Y^2(t)\rangle$ as projected onto the [010] (Y) and $[\bar{5}01]$ (X) directions by averaging over 3×10^5 independent KMC simulations at different temperatures ($T \in [700,1000]$ K). We then extracted the diffusion coefficients by using for both directions the one-dimensional Einstein relation $D_X=\lim_{t\to\infty}\langle X^2(t)\rangle/2t$ (an analogous expression holds for D_Y). In the KMC simulations, the initial atomic positions were randomly drawn from a Boltzmann distribution based on the minimum-energy values of Table I, while a few thousands extra thermalization steps were run before recording the trajectories. The diffusion coefficients are reported in Fig. 5 (lower panel), together with the mean square displacements at $T=800$ K (upper panel). As is clear from the figure, $D_X \sim D_Y$. In particular, the data are almost perfectly fitted by the Arrhenius relations

$$D_X(\mathrm{cm^2/s}) \sim 0.026(\mathrm{cm^2/s})e^{-\frac{0.62(\mathrm{eV})\times 11\,603(\mathrm{K/eV})}{T(\mathrm{K})}}$$

$$D_Y(\mathrm{cm^2/s}) \sim 0.032(\mathrm{cm^2/s})e^{-\frac{0.64(\mathrm{eV})\times 11\,603(\mathrm{K/eV})}{T(\mathrm{K})}}. \quad (2)$$

Thus, the effective barriers for diffusion in the $[\bar{5}01]$ and in the [010] directions turn out to be $E_{[\bar{5}01]}\sim 0.62$ eV and $E_{[010]}\sim 0.64$ eV, respectively. Our results, thus, quantitatively demonstrate that diffusion at the (105)RS surface tends to be isotropic, at variance with what occurs at the (001) surface.[32] The actual value of the effective diffusion barriers is also interesting, since it shows that diffusion at the (105)RS surface is as fast as diffusion along the fast direction (i.e., along the dimer rows) on a Ge(001) $c(4\times2)$ surface under a ~4% compressive strain,[25] i.e., under conditions resembling a Ge wetting layer on Si(001). Therefore, we conclude that adatom diffusion on the (105)RS surface is an easy process at experimental temperatures ($T\gtrsim700$ K), displaying typical diffusion coefficients (see Fig. 5) of the order of 10^{-6} cm^2/s.

In the present section we have presented hTST-based estimates of the diffusion coefficient, and KMC trajectories illustrating the typical diffusive behavior for an isolated Ge adatom on the Ge(105)RS surface. Here we recall that hTST provides excellent estimates of the rates whenever E_i is much

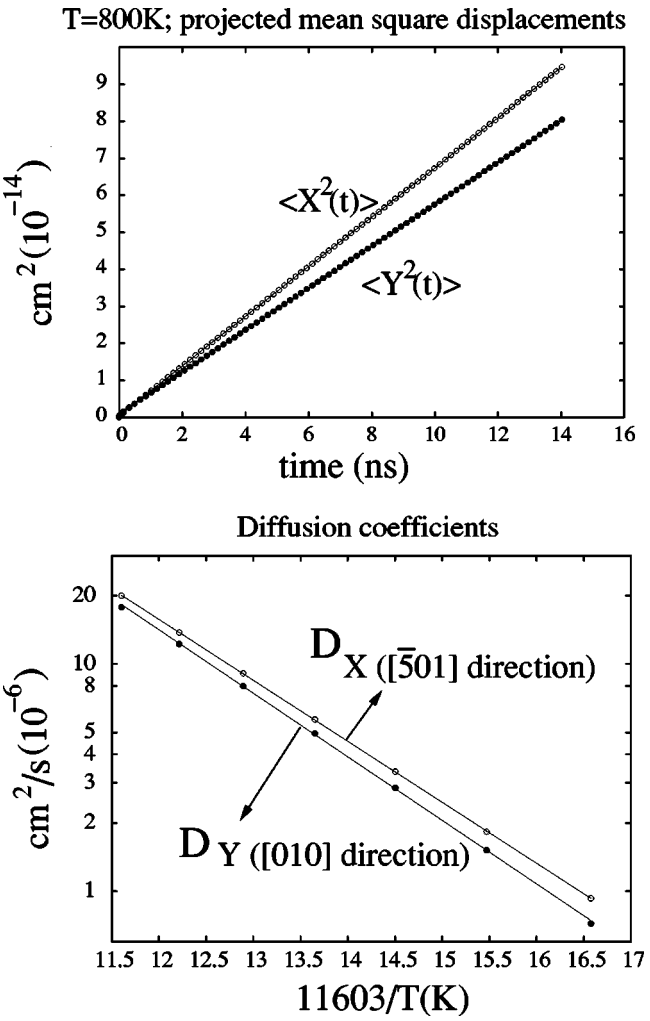

FIG. 5. Upper panel: mean square displacements along [010] (Y) and $[\bar{5}01]$ (X), as obtained by averaging over 3×10^5 independent KMC simulations at $T=800$ K. Lower panel: diffusion coefficients along the two directions. A logarithmic scale is used for the vertical axis. Solid lines represent best-fits using the Arrhenius law [Eq. (2)].

greater than the thermal energy (k_BT), so that the overall diffusive process can be considered as a sequence of rare, uncorrelated events. In practice, $E_i/(k_BT)$ ratios of the order of ~4–5, are sufficient to guarantee the validity of hTST.[15] At the highest temperature considered in our simulations (T=800 K) rates for events with barriers of ~0.3 eV or higher should therefore be estimated correctly, while, for lower barriers, deviations from hTST should be expected. Some mechanisms with very low activation energies were found, but they were shown to simply cause local motion around the HS structures, without producing any real diffusive event. The effective diffusion barrier for adatom motion, indeed, turned out to be $\gtrsim$0.6 eV, indicating that the set of relevant events leading to diffusion falls well within the validity range of hTST. Finally, we would like to point to the reader the work of Penev *et al.*,[33] where an approach alternative to KMC is used, yielding an analytical expression for the diffusion coefficient. In Ref. 33, however, the number of elementary mechanisms was much smaller than in the

TABLE III. Binding energies (eV) for the various adatom local minima computed at both $a_{\parallel}=a_{\mathrm{Ge}}$ and $a_{\parallel}=a_{\mathrm{Si}}$. Energy values are evaluated by subtracting the total energy of the various configurations to the energy of the clean surface, at the two different lattice parameters.

	A	*B*	*C*	*D*	*E*	*F*	*G*	*H*	*I*	*J*	*K*	*L*	*M*
a_{Ge}	−4.332	−4.510	−4.399	−4.503	−4.232	−4.047	−4.109	−4.187	−4.262	−3.978	−4.170	−4.142	−4.074
a_{Si}	−4.246	−4.524	−4.307	−4.535	−3.961	−4.028	−4.158	−4.234	−4.196	−4.082	−4.102	−3.989	−4.061

present case, and a direct extension of the their calculations to our system appears highly nontrivial.

IV. DIFFUSION UNDER COMPRESSIVE STRAIN

We have presented our results for adatom self-diffusion on Ge(105)RS, at the Ge lattice parameter ($a_{\parallel}=a_{\mathrm{Ge}}$). It is important to recall that in three-dimensional Ge dots on Si(001), the average lattice parameter changes along the dot, starting from a value close to the typical Si one at the base, and expanding towards a_{Ge}.[3] Therefore, the results reported in the previous section should be regarded as representative of diffusion at the pyramids facets close enough to the apex. In order to check whether compression significantly affects diffusion, we have repeated our calculations at $a_{\parallel}=a_{\mathrm{Si}}=5.431$ Å, i.e., by considering a ~4% compression of the in-plane lattice parameter, which should be representative of the typical situation encountered in the proximity of the pyramid base.[34] Since our aim here is simply to understand if the qualitative features (fast and isotropic diffusion) found for $a_{\parallel}=a_{\mathrm{Ge}}$ still hold, in repeating the calculations for $a_{\parallel}=a_{\mathrm{Si}}$ we tried to save some computational time. In particular, we did not perform the whole local-minima search described in Sec. II A. Simply, we reconverged at $a_{\parallel}=a_{\mathrm{Si}}$ the 13 nonequivalent minima position found for $a_{\parallel}=a_{\mathrm{Ge}}$. The relative energies (computed with respect to the best adsorption site *D* for $a_{\parallel}=a_{\mathrm{Si}}$, while site *B* was slightly favoured at $a_{\parallel}=a_{\mathrm{Ge}}$) can be found in the second row of Table I.

The results reported in Table I allow one to capture strain-related changes in energy differences among minima computed at the same lattice parameter. In order to directly compare the binding energy at the various sites for the two lattice-parameter values, we computed the difference between the total energy of the slab containing the adatom at a given site and the total energy of the clean surface (both terms being evaluated at the same $a_{\parallel}$ value). Results are reported in Table III.[35] The table shows that the trend in the adsorption energies vs lattice parameter depends on the actual site. While for most of the sites the energy for $a_{\parallel}=a_{\mathrm{Ge}}$ is lower than the corresponding one for $a_{\parallel}=a_{\mathrm{Si}}$, this is not what happens at the best adsorption sites (*B* and *D*) where compression seems to enhance stability. This energy lowering can be qualitatively explained in terms of bond stretching. In both *B* and *D* configurations the adatom binds to two HS atoms. For $a_{\parallel}=a_{\mathrm{Ge}}$ these bonds tend to be stretched. For istance, in minimum *B*, the length of the bond between the adatom and the HS atom on its right side (see the central panel of Fig. 2) is ~3.5% expanded with respect to the bulk distance. A similar expansion characterizes also the length of the bond between the adatom in *D* and the HS atom to its left (lower panel of Fig. 2). As a consequence, by reducing $a_{\parallel}$ to a_{Si} one enhances the stability of such bonds.

While common sense would suggest binding energies to be minima at the bulk lattice parameter (a_{Ge}), the observation of an opposite trend occurring at some sites is not new. Van de Walle *et al.*, already observed compression-enhanced adsorption sites stability on the Ge(001), $c(4\times2)$ reconstructed surface.[25] We believe that in both the present case and in Ref. 25, the odd trend in the binding-site energetics is linked to the complexity of the surface reconstruction, which is characterized by a local atomic configuration remarkably different with respect to the bulk one. While the total energy of an infinite substrate with a surface obviously reaches its minimum value at the bulk lattice parameter, in the presence of surface reconstructions involving major rebonding, additional isolated adatoms cannot be considered as representative building blocks for adding a new monolayer to the substrate. As a consequence, the energetics of the single adatom does not necessarily reflect the thermodynamic of the whole system. Additional work investigating lattice-parameter dependent ad dimers and ad islands binding energies is surely needed in order to further clarify this issue.

While at the lowest-energy minima (*B* and *D*), the lattice-parameter reduction does not cause major rearrangements, in some of the other configurations qualitative changes are observed when passing from $a_{\parallel}=a_{\mathrm{Ge}}$ to $a_{\parallel}=a_{\mathrm{Si}}$. For example, in minimum *A* the reduced lattice parameter prevents the previously discussed adatom-induced dimer breaking (compare the upper panel of Fig. 3 with Fig. 6) and, in turn, the formation of an additional bond between the adatom and the surface. As a consequence, the binding energy at site *A* decreases at $a_{\parallel}=a_{\mathrm{Si}}$ (see Table III). Somewhat similar changes are observed also at sites *C*, *E*, and *L*, and in all such cases the minima are deeper for $a_{\parallel}=a_{\mathrm{Ge}}$.

After reconverging the 13 nonequivalent minima configurations at $a_{\parallel}=a_{\mathrm{Si}}$, we also repeated the whole set of activation-energy calculations described in Sec. II B. In order to save computational time, saddle points were optimized using a $2\times3\times1$ grid of Monkhorst-Pack points. We verified for two saddle-point configurations that the use of a larger, $4\times5\times1$ grid, did not change in any significant way the estimate of the diffusion barrier. The various activation energies are reported in the second row of Table II. Comparing such values with the ones obtained at $a_{\parallel}=a_{\mathrm{Ge}}$ (first row of the same table), we notice that most (but not all) barriers are raised by the compressive-strain action, in qualitative agreement with the results of van de Walle *et al.* on Ge adatom diffusion on Ge(001).[25] KMC simulations, repeated using the whole set of the $a_{\parallel}=a_{\mathrm{Si}}$ results, confirmed this observation, leading to an estimate of $E_{[\bar{5}01]}\sim0.72$ eV (~0.1 eV higher than the result obtained at $a_{\parallel}=a_{\mathrm{Ge}}$) and $E_{[010]}\sim0.67$ eV (

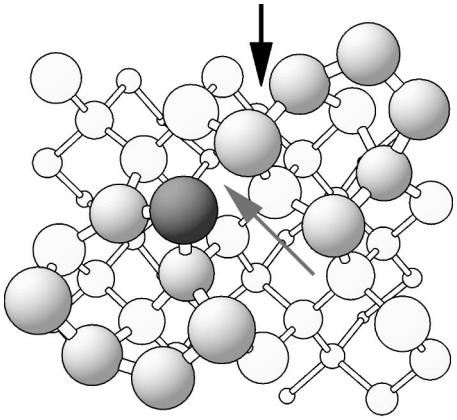

FIG. 6. Top view of the *A* adatom configuration, as optimized for $a_{\parallel}=a_{\mathrm{Si}}$. Atoms are displayed following the same criteria described in the caption of Fig. 2. The black arrow indicates the bond that for $a_{\parallel}=a_{\mathrm{Ge}}$ breaks (see the upper panel of Fig. 3), while the gray one is used to emphasize that no bonds are formed between the adatom and the gray atom of the HS structure, at variance with the $a_{\parallel}=a_{\mathrm{Ge}}$ case.

$\sim$0.03 eV higher than at $a_{\parallel}=a_{\mathrm{Ge}}$). It might be worth noticing that on fcc metal surfaces an opposite trend has been predicted,[36,37] demonstrating that the dependence of the adatom jump barrier on the lattice parameter is strongly system dependent.

To this end, a $\sim$4% compressive strain tends to slow down diffusion in both [010] and $[\bar{5}01]$ directions, the effect being more pronounced along the latter. Changes in barriers, however, are not particularly significant at the typical experimental temperatures, and the overall picture of fast and almost isotropic diffusion is likely to hold for any compressive strain in the range (4–0 %), i.e., along the whole Ge pyramid facet in Ge/Si(001) systems.

V. CONCLUSIONS: INFLUENCE ON PYRAMID GROWTH MODES

Ge three-dimensional islands grown on Si(001) are well known to display a bimodal behavior. The coexistence between small {105} pyramids and larger *domes* has been clearly demonstrated in two seminal experimental papers.[6,7] Recently, Seifert and co-workers[38] provided a simple explanation for the pyramid-to-dome transition: new {105} layers preferentially nucleate at the topmost regions of the pyramid facets, due to the lattice parameter expansion towards the Ge bulk value. Hence, material tends to accumulate in such regions, facilitating the formation of the steeper facets which characterize the dome geometry. A very detailed, atomic-scale evidence for such a transition path is provided in Ref. 39, where STM images demonstrate a progressive step bunching taking place close to the pyramids apex, eventually leading to the transformation between {105} and domelike steep facets. The above reported evidence suggests that pyramid growth proceeds from top to bottom: a critical nucleus is created at the topmost regions, while facets are completed afterwards by a fast step-flow process. In order to justify such an evidence, one needs to assume surface diffusion to be fast in the base-to-top ($[\bar{5}01]$) direction, since new material is observed to climb the facets and to easily reach the upper regions. The results presented in this paper provide a theoretical justification for such an assumption. Notice that, in the absence of the actual {105} facets reconstruction, a fast facet-climbing process would be hardly justified. Indeed, facets would display a staircaselike geometry, and motion towards the apex would involve a repeated (slow) step-crossing process. The model of Ref. 40 (published before the RS reconstruction was demonstrated to characterize the dots facets[9]) was based on this picture, and predicted a bottomside-up growth mode, at variance with the recent results of Refs. 38, 39, and 41.

In this work we have investigated adatom self-diffusion at the Ge(105) surface, reconstructed following the RS model. Based on *ab initio* estimates of various atomic diffusion paths and on KMC simulations, we have shown that diffusion at typical experimental temperatures is an easy process, almost equally fast along the $[\bar{5}01]$ and [010] directions, particularly relevant for modeling Ge pyramids growth on Si(001). In eliminating the typical step structures of the as-cut (105) surface, the RS reconstruction makes it easier for adatoms to reach the topmost regions of {105} Ge pyramids grown on Si(001), where nucleation of a new facet seems favored from a thermodynamic point of view. Hence, the present calculations provide theoretical support to the recent experimental evidences of a top-to-bottom pyramid growth mode. More work, however, is surely needed in order to build a satisfactory atomistic model of kinetics at Ge pyramids, including a comprehensive analysis of dimers and larger islands stability and mobility at the {105} facets.

ACKNOWLEDGMENTS

Computational support from the CINECA (INFM project "Iniziativa Calcolo Parallelo 2004") and CILEA (within the L-NESS enterprise) supercomputing facilities is gratefully acknowledged. L-NESS (Laboratory for Nanometric Epitaxial Structures on Silicon and Spintronics) is a joint research center of Politecnico di Milano and University of Milano-Bicocca. We wish to thank our student S. Cereda for technical support.

*Email address: francesco.montalenti@unimib.it

[1] Y. W. Mo, D. E. Savage, B. S. Swartzentruber, and M. G. Lagally, Phys. Rev. Lett. **65**, 1020 (1990).
[2] D. J. Eaglesham and M. Cerullo, Phys. Rev. Lett. **64**, 1943 (1990).
[3] V. A. Schukin and D. Bimberg, Rev. Mod. Phys. **71**, 1125 (1999).
[4] B. Voigtländer, Surf. Sci. Rep. **43**, 127 (2001).
[5] A. G. Cullis, MRS Bull. **21**, 21 (1996).
[6] G. Medeiros-Ribeiro, A. M. Bratkovski, T. I. Kamins, D. A. A. Ohlberg, and R. S. Williams, Science **279**, 353 (1998).
[7] F. M. Ross, R. M. Tromp, and M. C. Reuter, Science **286**, 1931 (1999).
[8] K. E. Khor and S. D. Sarma, J. Vac. Sci. Technol. B **15**, 1051 (1997).
[9] P. Raiteri, D. B. Migas, L. Miglio, A. Rastelli, and H. von Känel, Phys. Rev. Lett. **88**, 256103 (2002).
[10] Y. Fujikawa, K. Akiyama, T. Nagao, T. Sakurai, M. G. Lagally, T. Hashimoto, Y. Morikawa, and K. Terakura, Phys. Rev. Lett. **88**, 176101 (2002).
[11] T. Hashimoto, Y. Morikawa, Y. Fujikawa, T. Sakurai, M. G. Lagally, and K. Terakura, Surf. Sci. **513**, L445 (2002).
[12] D. B. Migas, S. Cereda, F. Montalenti, and L. Miglio, Surf. Sci. **556**, 121 (2004).
[13] V. B. Shenoy, C. V. Ciobanu, and L. B. Freund, Appl. Phys. Lett. **81**, 364 (2002).
[14] C. V. Ciobanu, V. B. Shenoy, C. Z. Wang, and K. M. Ho, Surf. Sci. **544**, L715 (2003).
[15] T. Ala-Nissila, R. Ferrando, and S. C. Ying, Adv. Phys. **51**, 949 (2002).
[16] T. Michely and J. Krug, *Islands, Mounds and Atoms* (Springer, Berlin, 2004).
[17] P. Hänggi, P. Talkner, and M. Borkovec, Rev. Mod. Phys. **62**, 251 (1990).
[18] G. Kresse and J. Hafner, Phys. Rev. B **49**, 14 251 (1994).
[19] G. Kresse and J. Furthmüller, Comput. Mater. Sci. **6**, 15 (1996).
[20] D. Vanderbilt, Phys. Rev. B **41**, 7892 (1990).
[21] G. Kresse and J. Hafner, J. Phys.: Condens. Matter **6**, 8245 (1994).
[22] J. P. Perdew and A. Zunger, Phys. Rev. B **23**, 5048 (1981).
[23] H. Jònsson, G. Mills, and K. W. Jacobsen, in *Classical and Quantum Dynamics in Condensed Phase Simulations*, edited by B. J. Berne, G. Ciccotti, and D. F. Coker (World Scientific, Singapore, 1998), p. 383.
[24] G. Henkelman, B. P. Uberuaga, and H. Jónsson, J. Chem. Phys. **113**, 9901 (2000).
[25] A. van de Walle, M. Asta, and P. W. Voorhees, Phys. Rev. B **67**, 041308(R) (2003).
[26] G. Henkelman, Ph.D. thesis, University of Washington, Seattle, 2001.
[27] A. P. Smith and H. Jónsson, Phys. Rev. Lett. **77**, 1326 (1996).
[28] P. Kratzer and M. Scheffler, Phys. Rev. Lett. **88**, 036102 (2002).
[29] A. B. Bortz, M. H. Kalos, and J. L. Lebowitz, J. Comput. Phys. **17**, 10 (1975).
[30] A. F. Voter, Phys. Rev. B **34**, 6819 (1986).
[31] K. A. Fichthorn and W. H. Weinberg, J. Chem. Phys. **95**, 1090 (1991).
[32] Y. W. Mo, J. Kleiner, M. B. Webb, and M. G. Lagally, Phys. Rev. Lett. **66**, 1998 (1991).
[33] E. Penev, S. Stojković, P. Kratzer, and M. Scheffler, Phys. Rev. B **69**, 115335 (2004).
[34] During Ge deposition on Si(001), the Si substrate forces the atoms of the Ge wetting layer at the Si lattice parameter in (001) planes, resulting in a ~4% compressive strain. For simplicity, here we assume that the same in-plane reduction takes place also on the (105) planes characterizing Ge {105} pyramid facets close to the island base. The small miscut angle (~11.31°) should make this assumption sufficiently accurate for the present goal of qualitatively estimating the effect of strain on diffusion.
[35] The results in Table I can be inferred from Table III. However, we preferred to keep Table I in order to make it easier to estimate the activation energies for the whole set of diffusion paths.
[36] C. Ratsch, A. P. Seitsonen, and M. Scheffler, Phys. Rev. B **55**, 6750 (1997).
[37] J. A. Sprague, F. Montalenti, B. P. Uberuaga, J. D. Kress, and A. F. Voter, Phys. Rev. B **66**, 205415 (2002).
[38] V. Zela, I. Pietzonka, T. Sass, C. Thelander, S. Jeppesen, and W. Seifert, Physica E (Amsterdam) **13**, 1013 (2002).
[39] F. Montalenti, P. Raiteri, D. B. Migas, H. Von Känel, A. Rastelli, C. Manzano, G. Costantini, U. Denker, O. G. Schmidt, K. Kern, and L. Miglio, Phys. Rev. Lett. **93**, 216102 (2004).
[40] M. Kästner and B. Voigtländer, Phys. Rev. Lett. **82**, 2745 (1999).
[41] J. Johansson and W. Seifert, J. Cryst. Growth **234**, 139 (2002).